PNAS RESEARCH ARTICLE | IMMUNOLOGY AND INFLAMMATION

Disruption of the ZFP574–THAP12 complex suppresses B cell malignancies in mice

Xue Zhong[a], James J. Moresco[a], Jeffrey A. SoRelle[b], Ran Song[a], Yiao Jiang[a], Mylinh T. Nguyen[c], Jianhui Wang[a], Chun Hui Bu[a], Eva Marie Y. Moresco[a], Bruce Beutler[a,1], and Jin Huk Choi[a,d,1]

Contributed by Bruce Beutler; received May 8, 2024; accepted June 24, 2024; reviewed by Christopher C. Goodnow and Josef T. Prchal

Despite the availability of life-extending treatments for B cell leukemias and lymphomas, many of these cancers remain incurable. Thus, the development of new molecular targets and therapeutics is needed to expand treatment options. To identify new molecular targets, we used a forward genetic screen in mice to identify genes required for development or survival of lymphocytes. Here, we describe *Zfp574*, an essential gene encoding a zinc finger protein necessary for normal and malignant lymphocyte survival. We show that ZFP574 interacts with zinc finger protein THAP12 and promotes the G1-to-S-phase transition during cell cycle progression. Mutation of ZFP574 impairs nuclear localization of the ZFP574–THAP12 complex. ZFP574 or THAP12 deficiency results in cell cycle arrest and impaired lymphoproliferation. Germline mutation, acute gene deletion, or targeted degradation of ZFP574 suppressed Myc-driven B cell leukemia in mice, but normal B cells were largely spared, permitting long-term survival, whereas complete lethality was observed in control animals. Our findings support the identification of drugs targeting ZFP574–THAP12 as a unique strategy to treat B cell malignancies.

ZFP574 | THAP12 | cell cycle | B cell malignancies | ENU

Significance

This work establishes the protein complex ZFP574–THAP12 as a promising molecular target for the treatment of B cell cancers. We show that zinc finger proteins ZFP574 and THAP12 regulate cell cycling to support blood cell development in mice. Acute gene deletion or targeted degradation of ZFP574 eliminated leukemic B cells preferentially over nonmalignant B cells in vivo.

More than 1,500 zinc finger proteins exist in humans, among which C2H2 motif zinc finger proteins are the most abundant type (~46%). ZFP574 is a zinc finger protein containing 20 C2H2 zinc finger motifs. A single 900-amino-acid (aa) isoform exists in mice, while in humans two isoforms are generated by alternative splicing (896 and 985 aa). The amino acid sequences of mouse and human ZFP574 (896-aa isoform) are 93.6% identical. ZFP574 is essential for life, yet little is known of its physiological functions during development or in adulthood. Up-regulated gene expression or increased gene copy number of human *ZFP574* in colon and ovarian cancers has been reported, suggesting that *ZFP574* may be an oncogene, although no functional studies were conducted to test this hypothesis (1, 2). Differentiation of human embryonic stem cells induced by retinoic acid treatment resulted in hypermethylation of *ZFP574* on CpG sites and its transcriptional downregulation (3). Finally, the zebrafish C2H2 zinc finger protein Rumba, which is orthologous to several human genes including *ZNF212, ZNF526, ZFP574, ZFP662,* and *ZFP667* (4), was implicated in hematopoietic stem/progenitor cell maintenance (5).

The human THAP zinc finger family consists of 12 members (7 in mice), which all harbor an N-terminal C2CH zinc finger (THAP domain) with sequence-specific DNA-binding activity. THAP domains bind to DNA by a bipartite interaction with the DNA major and minor grooves (6). THAP proteins exhibit different DNA-binding specificities due to divergence of the residues that contact DNA in different THAP domains (7, 8). Most THAP proteins contain both a coiled-coil domain and a host cell factor-1 (HCF-1) binding domain (HBM) that mediates interaction with HCF-1, a ubiquitous transcriptional coregulator that recruits chromatin modifiers. However, THAP12 is one of the two THAP proteins with neither a coiled-coil nor an HBM domain (9). There are two human THAP12 isoforms (761-aa and 696-aa) and one mouse THAP12 isoform (758-aa), with 94.6% amino acid identity between the human 761-aa and mouse 758-aa proteins. Earlier work showed that a truncated form of THAP12 (also known as 52 kDa repressor of the inhibitor of the protein kinase: $p52^{rIPK}$) functions as an indirect activator of the interferon-induced serine/threonine protein kinase PKR in yeast (10). THAP12 was also reported to mediate the type I IFN response by protecting RIG-I (retinoic acid inducible gene-I) from ubiquitin-dependent degradation in HEK293FT cells (11). However, the physiological processes supported by wild-type THAP12 remain unknown.

We identified a viable *N*-ethyl-*N*-nitrosourea (ENU)-induced missense allele of *Zfp574* in a forward genetic screen for impaired lymphocyte development, maintenance, or function in C57BL/6J mice. Here, we show that ZFP574 and THAP12 form a complex that supports

Author affiliations: [a]Center for the Genetics of Host Defense, University of Texas Southwestern Medical Center, Dallas, TX 75390; [b]Department of Pathology, University of Texas Southwestern Medical Center, Dallas, TX 75390; [c]Department of Biochemistry, University of Texas Southwestern Medical Center, Dallas, TX 75390; and [d]Department of Immunology, University of Texas Southwestern Medical Center, Dallas, TX 75390

Author contributions: X.Z., B.B., and J.H.C. designed research; X.Z., J.J.M., J.A.S., R.S., Y.J., J.W., and J.H.C. performed research; M.T.N. and C.H.B. contributed new reagents/analytic tools; X.Z., J.J.M., C.H.B., and J.H.C. analyzed data; and X.Z., E.M.Y.M., B.B., and J.H.C. wrote the paper.

Reviewers: C.C.G., Garvan Institute of Medical Research; and J.T.P., The University of Utah.

The authors declare no competing interest.

[1]To whom correspondence may be addressed. Email: bruce.beutler@utsouthwestern.edu or jin.choi@utsouthwestern.edu.

This article contains supporting information online at https://www.pnas.org/lookup/suppl/doi:10.1073/pnas.2409232121/-/DCSupplemental.

Published July 24, 2024.

cell cycling. Disruption of ZFP574–THAP12 complex function broadly impaired hematopoiesis and severely disrupted leukemic cell proliferation.

Results

Immunodeficiency Caused by a Single Nucleotide Change in the Essential Gene *Zfp574*. Forward genetic studies begin by creating phenotypic variations in model systems using germline mutagens. Researchers then identify causative mutations and define the functions of genes in specific biological phenomena. Our approach involves inducing single nucleotide changes in the mouse germline genome using ENU, while keeping surveillance over normal physiological processes that interest us. To identify genes required for the development or survival of lymphocytes, we screened mice carrying ENU-induced mutations for altered immune cell frequencies in the peripheral blood or diminished antibody responses to immunization. Three siblings from a single pedigree exhibited low percentages of B cells in the peripheral blood (Fig. 1*A*) and diminished T cell–dependent (TD) antibody responses to recombinant Semliki Forest virus-encoded β-galactosidase (rSFV-βgal; Fig. 1*B*) (12). We termed the phenotype *glue*. By automated meiotic mapping, a method that analyzes genotype–phenotype associations in single or multiple pedigrees (13), the *glue* phenotype correlated with cosegregating mutations in *Zfp574* and *Ceacam3* (Fig. 1*C*). *Zfp574* had no known function in immunity. *Ceacam3* encodes CEA cell adhesion molecule 3, known to function in phagocytosis of bacterial pathogens (14). To determine which mutation was responsible for the *glue* phenotype, we generated CRISPR/Cas9-mediated mutations in *Zfp574* and *Ceacam3* in C57BL/6J mice, each on a clean background and reproducing the original ENU-induced single nucleotide changes causing the amino acid changes histidine 512 to glutamine in *Zfp574* (H512Q; Fig. 1*D*) or serine 35 to threonine in *Ceacam3* (S35T; *SI Appendix*, Fig. S1). No effects on lymphopoiesis or adaptive immune function were observed in *Ceacam3* mutant mice (*SI Appendix*, Fig. S1). The H512Q mutation in *Zfp574* was solely responsible for the immune phenotypes observed in *glue* mice (Fig. 1 *E* and *H*). Decreased frequencies of B-1 B cells, T cells, and reduced T cell–independent (TI) antibody responses to NP-Ficoll were also detected (Fig. 1 *F*, *G*, and *I*). Crosses of heterozygotes carrying a CRISPR/Cas9-targeted null allele of *Zfp574* yielded neither homozygous null pups nor $Zfp574^{H512Q/-}$ compound heterozygotes, indicating that complete ablation of *Zfp574* causes prenatal lethality ($P < 0.001$; *SI Appendix*, Table S1); also that the $Zfp574^{H512Q}$ allele is hypomorphic, but the encoded protein retains some function.

To test the intrinsic functionality of $Zfp574^{H512Q/H512Q}$ B cells, we adoptively transferred them to sublethally irradiated WT hosts. Mutant B cell homeostatic proliferation was impaired and apoptosis was increased in the lymphodepleted recipients (Fig. 1 *J* and *K*). We also tested $Zfp574^{H512Q/H512Q}$ B cell function in vitro. LPS- and IL-4-induced CSR to IgG1 and cell division were decreased in $Zfp574^{H512Q/H512Q}$ B cells compared to wild-type cells (Fig. 1*L*). Consistent with this result, naive *Zfp574* mutant mice failed to retain the capacity to produce basal levels of major immunoglobulin isotypes in serum except IgE (Fig. 1*M*). Furthermore, cell cycle analysis of naive B cells during LPS- and IL-4-induced activation showed an increased frequency of $Zfp574^{H512Q/H512Q}$ cells arrested in G0/G1 phases with concomitant reduction of cells in S phase compared to wild-type cells (Fig. 1*N*). Collectively, these results suggest that ZFP574 is indispensable for B cell development, function, proliferation, and cell cycle progression.

ZFP574 Functions Within Hematopoietic Stem and Progenitor Cell (HSPC) Populations to Support Normal Hematopoiesis. Homozygosity for the viable $Zfp574^{H512Q}$ allele caused pancytopenia with macrocytic anemia (*SI Appendix*, Fig. S2). To characterize the hematopoietic defects caused by *Zfp574* deficiency, we tried to generate mice in which *Zfp574* was conditionally deleted in hematopoietic cells using a floxed allele of *Zfp574* ($Zfp574^{f/f}$). However, Vav-iCre-driven *Zfp574* deletion in the hematopoietic compartment of zygotes also resulted in embryonic lethality ($P = 0.002$; *SI Appendix*, Table S1). Therefore, we crossed $Zfp574^{f/f}$ mice with UBC-Cre-ERT2 transgenic mice, which express a tamoxifen-inducible Cre transgene throughout the body. We transplanted a 1:1 mixture of UBC-Cre-ERT2;$Zfp574^{f/f}$ (CD45.2) and congenic wild-type (C57/BL6J; CD45.1) BM cells into lethally irradiated CD45.1 recipients. At 12 wk posttransplant, recipients were injected with either tamoxifen or vehicle control. In contrast to vehicle control recipients, mice that received tamoxifen to induce Cre-mediated *Zfp574* deletion showed rapid depletion of all HSPC populations derived specifically from UBC-Cre-ERT2;$Zfp574^{f/f}$ (CD45.2) BM (Fig. 2*A* and *SI Appendix*, Fig. S3). Progenitor cell populations (multipotent progenitor: MPP, lymphoid-primed multipotent progenitor: LMPP, common lymphoid progenitor: CLP, common myeloid progenitor: CMP, megakaryocyte-erythroid progenitor: MEP, and granulocyte-macrophage progenitor: GMP) were more severely affected by *Zfp574* deletion than HSCs. Consistent with these findings, tamoxifen-induced deletion of *Zfp574* throughout the body in adult mice fully reproduced the hematopoietic phenotype observed in germline *Zfp574* mutant mice including pan-cytopenia and anemia (Fig. 2*B*). These results indicate that ZFP574 functions beginning in HSPC populations to support normal hematopoiesis.

Identification of a ZFP574–THAP12 Complex that Controls Cell Cycle Progression. ZFP574 contains 20 C2H2 zinc fingers, a classical DNA-binding module, and no other notable functional domains (Fig. 1*D*). To gain insight into the mechanisms of ZFP574, we performed mass spectrometry (MS)-based interactome analysis. Immunoprecipitates prepared from a mouse T lymphoblast cell line, EL4, stably expressing FLAG-tagged ZFP574 contained THAP12 and multiple ribosomal proteins as putative interactors (*SI Appendix*, Fig. S4 *A–C* and Dataset S1). Reverse IP-MS analysis using EL4 T cells expressing THAP12-FLAG also identified ZFP574 as a primary binding partner of THAP12 (*SI Appendix*, Fig. S4 *A, B,* and *D* and Dataset S1). Since no ZFP574 antibodies are commercially available, we generated mice in which a 3X-FLAG tag was appended to the C terminus of endogenous ZFP574 by CRISPR-based knock-in both on a wild-type and mutant (H512Q) background. In splenic B cells from wild-type *Zfp574*-3X-FLAG knock-in mice, ZFP574 immunoprecipitated THAP12, the sole endogenous interactor with ZFP574 in B cells in two independent experiments (Fig. 3*A* and Dataset S2).

Since homozygosity for a null mutation of *Thap12* (15), or for either of two ENU-induced *Thap12* nonsense mutations in our collection, resulted in preweaning lethality in mice, we knocked out *Thap12* in EL4 cells, a T lymphoblastic lymphoma cell line, using CRISPR/Cas9. *Thap12* deficiency caused severe defects in cell growth and in G1 to S phase transition (Fig. 3 *B* and *C*) similar to those observed in $Zfp574^{H512Q/H512Q}$ B cells (Fig. 1*N*), supporting the physiological relevance of their interaction.

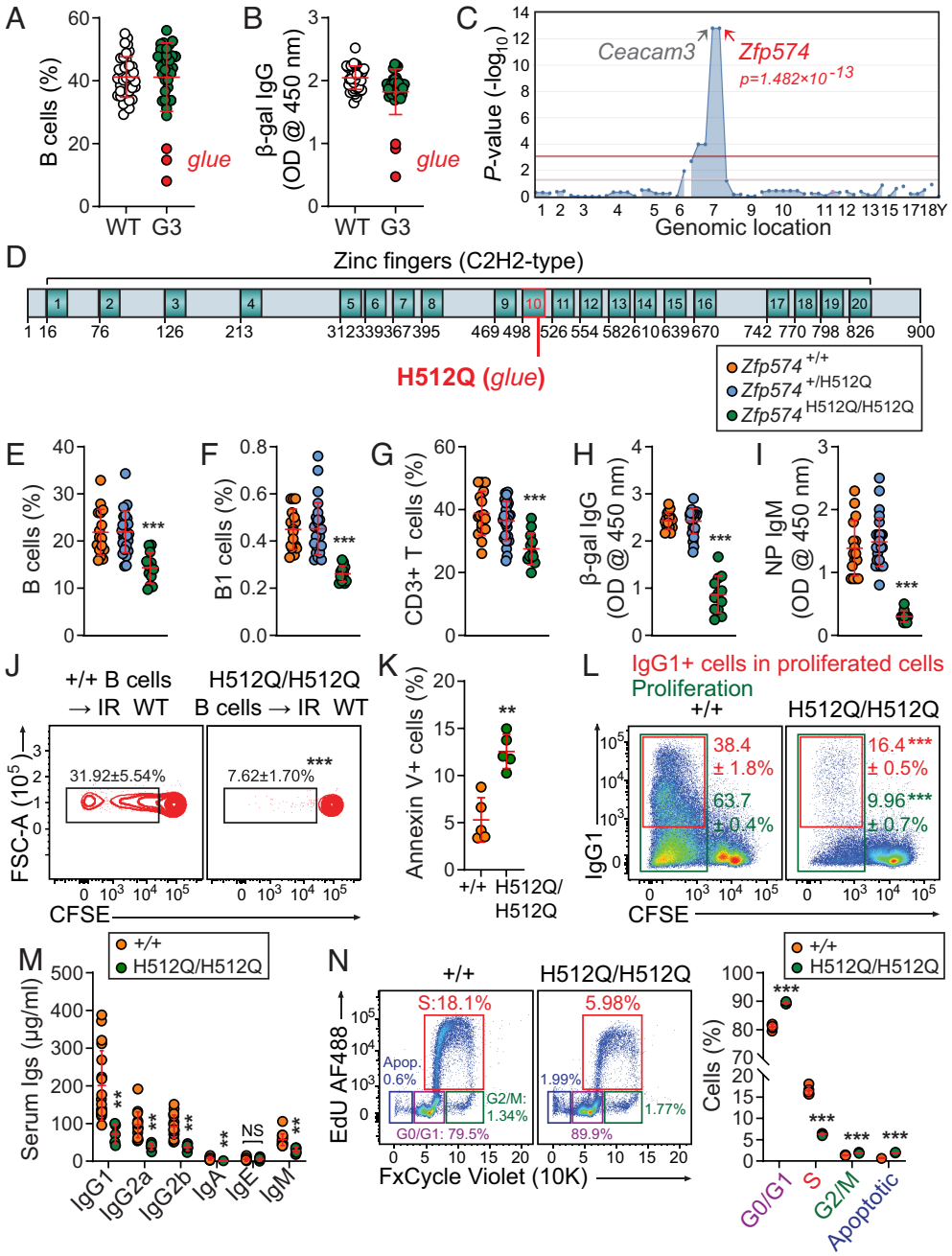

Fig. 1. A heritable lymphopenia caused by a viable mutation in *Zfp574*. (*A* and *B*) Frequency of B cells in the peripheral blood (*A*) and TD antibody response after immunization with a recombinant SFV vector encoding the model antigen, β-gal (rSFV-βGal) (*B*) of third-generation descendants (G3; the *glue* pedigree) of a single ENU-mutagenized male mouse (G1). Red, G3 mice homozygous for the *Zfp574* mutation; green, G3 mice homozygous for the *Zfp574* reference allele; white, WT C57BL/6J mice. (*C*) Manhattan plot showing -$\log_{10}$ *P*-values (*y* axis) plotted vs. the chromosomal positions of all mutations (*x* axis) identified in the G1 founder of the *glue* pedigree. (*D*) Protein domains of mouse ZFP574. The *glue* mutation, which results in histidine 512 to glutamine (H512Q) substitution, is indicated in red. Zinc finger motifs are indicated by green rectangles. (*E*–*G*) Frequency of B cells (*E*), B1 B cells (*F*), and T cells (*G*) in the peripheral blood from 12-wk-old mice with the indicated genotype for *Zfp574*. (*H* and *I*) TD (*H*) or TI (*I*) antibody responses in mice with the indicated genotype following immunization with rSFV-βGal or NP-Ficoll, respectively. (*J*) Impaired homeostatic expansion of *Zfp574* mutant B cells. $Zfp574^{+/+}$ and $Zfp574^{H512Q/H512Q}$ splenic B cells (CD45.2) were isolated and labeled with CFSE. Dye-labeled cells were injected into sublethally irradiated congenic wild-type (8.5 Gy, IR WT; CD45.1) recipients. Frequency of proliferated dye-labeled B cells in the spleens of recipients 14 d after adoptive transfer is shown. (*K*) Annexin V staining of donor-derived B cells in the spleen of recipient mice. (*L*) Class switch recombination (CSR) to IgG1 96 h poststimulation of splenic naive B lymphocytes with LPS and IL-4 in vitro. Proliferation of naive B cells was monitored by CFSE dilution. (*M*) Concentration of immunoglobulins in the serum of naive mice. (*N*) Cell cycle analysis of splenic naive B cells during LPS and IL-4 induced CSR. Numbers adjacent to outlined areas indicate percent cells in each (*J*, *L*, and *N*). Each symbol represents an individual mouse (*A*, *B*, *E*–*I*, *K*, *M*, and *N*). *P*-values were determined by one-way ANOVA with Dunnett's multiple comparisons (*E*–*I*) or Student's *t* test (*J*–*N*). Data are representative of one (*A* and *B*) or two independent experiments with 3 to 26 mice per genotype (*E*–*K* and *M*) or 5 to 6 technical replicates per group (*L* and *N*). Error bars indicate SD. $^{**}P < 0.01$; $^{***}P < 0.0001$; NS, not significant with $P > 0.05$.

Importantly, coimmunoprecipitation assays showed that the interaction between wild-type ZFP574 and THAP12 was unaltered by the H512Q mutation in ZFP574 (Fig. 3*D*). We mapped the regions of ZFP574 and THAP12 necessary for their interaction by coimmunoprecipitation of tagged proteins from HEK293T cells. THAP12 aa 150 to 360 contained the residues necessary for interaction with ZFP574, with the N-terminal boundary of the required region sharply defined at aa 151 (*SI Appendix*, Fig. S5 *A* and *B*). The C-terminal boundary of the required region lies between aa 209 and 359; no binding residues appear to be

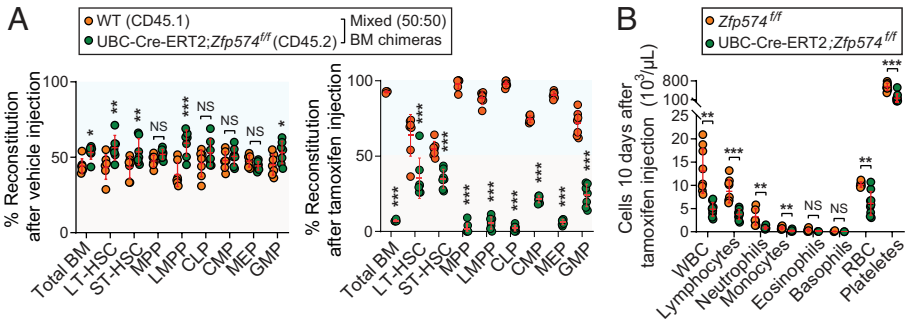

Fig. 2. A cell-intrinsic effect of acute *Zfp574* deletion on hematopoiesis. (*A*) Effects of acute *Zfp574* deletion in HSPCs in competitive BM chimeras. A 1:1 mixture of UBC-Cre-ERT2;*Zfp574*$^{f/f}$ BM (CD45.2) and congenic WT BM (C57BL/6J; CD45.1) cells was injected into lethally irradiated wild-type CD45.1 recipients. Twelve weeks after BM transplantation, recipients were administered with tamoxifen or vehicle control. On day 10 after tamoxifen or vehicle control administration, donor chimerism levels in BM HSPCs were assessed using congenic CD45 markers. (*B*) A complete blood count test in *Zfp574*$^{f/f}$ and UBC-Cre-ERT2;*Zfp574*$^{f/f}$ mice 10 d after tamoxifen administration. Each symbol represents an individual mouse (*A* and *B*). *P*-values were determined by Student's *t* test. Data are representative of two (*A*) or three (*B*) independent experiments with 7 to 9 mice per genotype. Error bars indicate SD. **P* < 0.05; ***P* < 0.01; ****P* < 0.0001. NS, not significant with *P* > 0.05.

C-terminal to aa 360. In ZFP574, zinc finger motifs 5 to 11 (aa 312 to 548) were necessary for interaction with THAP12 (*SI Appendix*, Fig. S5 *A* and *C*).

As mentioned, earlier work suggested that THAP12 may be an indirect activator of PKR signaling that can induce apoptosis as part of the antiviral or stress response by suppressing protein synthesis (10). However, we ruled out PKR activation as a cause of the ZFP574-THAP12-associated immunodeficiency by generating double mutant *Zfp574*$^{H512Q/H512Q}$;*Pkr*$^{-/-}$ mice and observing no rescue of lymphocyte deficiencies, anemia, and lymphocyte functional impairments caused by homozygous *Zfp574*^{H512Q} mutation (*SI Appendix*, Fig. S6).

AlphaFold (16) predicted structure of ZFP574 showed that histidine 512, which is part of the 10th zinc finger motif, is positioned in an α-helix and not involved in Zn^{2+} binding. Because Zn^{2+} coordination is likely to be unaffected, we expect that the C2H2 zinc finger fold is intact in the ZFP574^{H512Q} mutant protein. Consistent with this prediction, we detected similar expression levels of FLAG-tagged ZFP574^{WT} and ZFP574^{H512Q} in TCL of B and T cells from *Zfp574*-3X-FLAG knock-in mice (Fig. 3*E*).

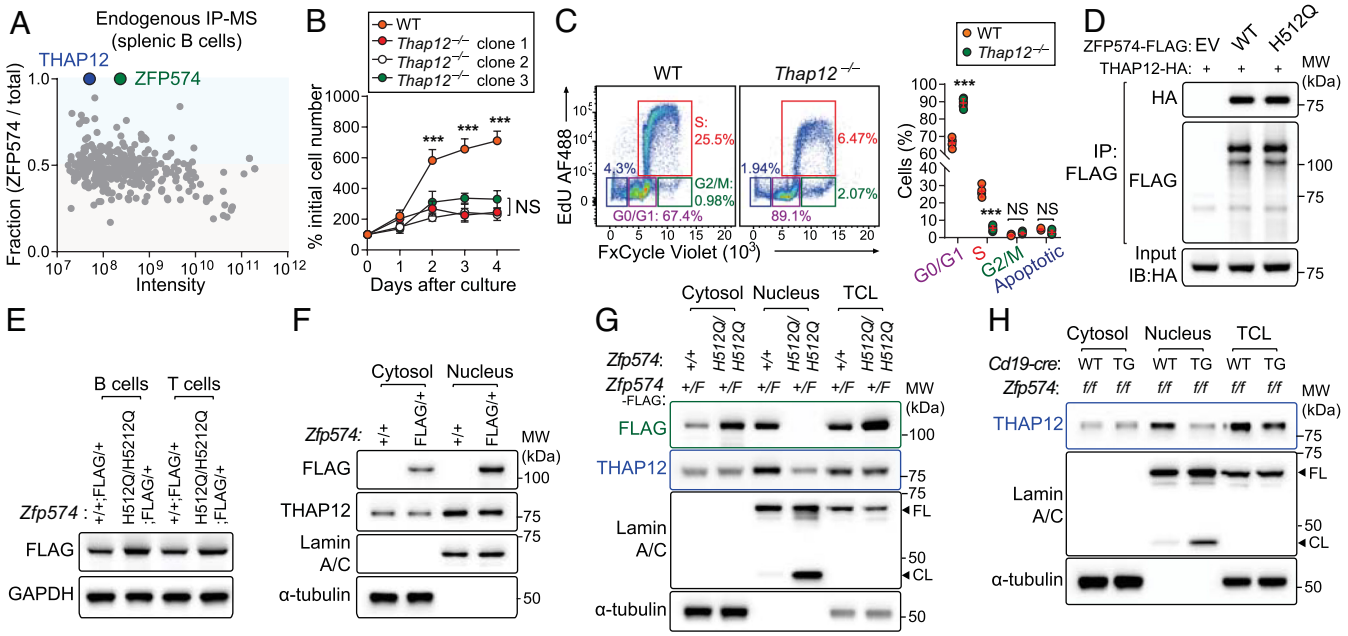

Fig. 3. Identification of a ZFP574–THAP12 complex that controls cell cycle progression. (*A*) ZFP574 interactors identified by MS analysis of proteins coimmunoprecipitated with ZFP574 from lysates of splenic B cells isolated from *Zfp574*-3X-FLAG knock-in mice (ZFP574 IP) or wild-type littermates (control IP). Relative protein abundance calculated using precursor ion intensities (abundance in ZFP574 IP ÷ sum of abundances in ZFP574 and control IP) is plotted on the *y* axis. y = 0.5 indicates equivalent abundance in the ZFP574 IP and control IP. y > 0.5 indicates enrichment in the ZFP574 IP, with y = 1 indicating that the protein was exclusively detected in the ZFP574 IP. *X* axis values represent the precursor ion intensity detected by MS. Data shown are combined from two independent MS analyses (n = 2 IP/genotype). (*B* and *C*) Growth curve (*B*) and cell cycle analysis (*C*) of *Thap12*$^{-/-}$ and parental wild-type EL4 cells. (*D*) The H512Q mutation in ZFP574 does not impair interaction with THAP12. HA-tagged THAP12, FLAG-tagged ZFP574^{WT}, or FLAG-tagged ZFP574^{H512Q} were each expressed in HEK293T cells. Cell lysates with the indicated protein expression were mixed and subsequently immunoprecipitated using anti-FLAG M2 agarose beads and immunoblotted with antibodies against HA or FLAG. EV: Empty vector. (*E*) Expression of endogenous FLAG-tagged ZFP574^{WT} or ZFP574^{H512Q} in whole cell lysates of splenic pan B and T cells from mice with the indicated genotype. GAPDH was used as a loading control. (*F*) Immunoblot analysis of subcellular fractions isolated from splenic B cells of *Zfp574*-3X-FLAG knock-in mice and wild-type littermates. (*G* and *H*) Immunoblot analysis of subcellular fractions or total cell lysates (TCL) of splenic B cells from *Zfp574*-3X-FLAG knock-in mice on a wild-type or *Zfp574*$^{H512Q/H512Q}$ background (*G*), or from mice in which *Zfp574* was conditionally deleted in B cells (Cd19-Cre;*Zfp574*$^{f/f}$) or littermate control mice (*Zfp574*$^{f/f}$; *H*). Expression of lamin A/C or α-tubulin were used as loading controls for the nucleus or cytosol, respectively. FL: full-length lamin A/C, CL: cleaved lamin A/C fragment. *P*-values were determined by one-way ANOVA with Dunnett's multiple comparisons (*B*) or Student's *t* test (*C*). Data are representative of two (*A* and *D*–*F*), three (*B*, *C*, and *G*), or five (*H*) independent experiments. Error bars indicate SD. ****P* < 0.001; NS, not significant with *P* > 0.05.

ZFP574^{WT} and THAP12 were expressed both in the cytoplasm and nucleus of splenic B cells, with relatively higher levels in the nucleus (Fig. 3*F*). Since the H512Q mutation in ZFP574 did not affect cellular protein abundance or its binding to THAP12, we examined the effect of the mutation or of ZFP574 deficiency on the intracellular localization of the protein complex. Although ZFP574^{H512Q} was more abundant than ZFP574^{WT} in TCL and cytosolic fractions of B cells, ZFP574^{H512Q} was greatly reduced compared to ZFP574^{WT} in nuclear fractions of the same B cells (Fig. 3*G*). Furthermore, an obvious decline in the nuclear abundance of THAP12, but not its total or cytosolic levels, was also found in *Zfp574* mutant or deficient B cells (Fig. 3 *G* and *H*). The reduction of ZFP574–THAP12 levels in the nucleus was associated with signs of cell death and nuclear dysregulation as indicated by increased proteolysis of Lamin A/C (Fig. 3 *G* and *H*). Our findings suggest that ZFP574 plays an essential role in nuclear localization of THAP12 and that reduced nuclear ZFP574–THAP12 levels may impair lymphocyte survival and cell cycle progression.

Germline Mutation or Acute Deletion of *Zfp574* Suppresses Mouse Models of Leukemia. Numerous cell cycle inhibitors are used as chemotherapy for cancers (17). Since the ZFP574–THAP12 complex is necessary for cell cycling in B cells and T cells, we hypothesized that it could be targeted to treat B cell malignancies. We therefore tested the effect of ZFP574 disruption in a Myc-driven B cell lymphoma and acute lymphocytic leukemia model. Mice with transgenic Myc expression driven by the IgH enhancer (Eμ-Myc^{TG}) invariably develop spontaneous pre-B cell leukemias and lymphomas presenting as lymphadenopathy early in life (median 9 wk of age) (18). Homozygosity for the *Zfp574*^{H512Q} allele significantly reduced the frequencies of B220^{low} leukemic pre-B cells in blood (Fig. 4*A*; Eμ-Myc^{TG};+/+: 40.54±18.7% vs. Eμ-Myc^{TG};*H512Q/H512Q*: 0.41±0.13%; $P < 0.0001$), prevented lymphoblast formation (Fig. 4 *B* and *C*), and lymphadenopathy (*SI Appendix*, Fig. S7) driven by Eμ-Myc^{TG}. Moreover, all Eμ-Myc^{TG};*H512Q/H512Q* mice (7/7) remained alive with no signs of leukemia for over a year (Fig. 4*D*), when all Eμ-Myc^{TG};+/+ mice (28/28) died by 25 wk of age (median survival: 117 d). Mice carrying both the Eμ-Myc transgene and a human BCL2 transgene driven by the IgH enhancer (Eμ-Bcl2^{TG}) develop a more aggressive primitive B cell leukemia by 5 wk of age (19). In these double transgenic mice, homozygosity for the *Zfp574*^{H512Q} allele substantially extended median survival time (Fig. 4*E*; Eμ-Myc^{TG};Eμ-Bcl2^{TG};+/+: 54 d vs. Eμ-Myc^{TG};Eμ-Bcl2^{TG};*H512Q/H512Q*: 113 d; $P < 0.001$), although it did not ultimately prevent death from leukemia.

We explored the effect on established B cell leukemia of acute Cre-mediated *Zfp574* deletion. We used a BM transplantation (BMT) approach in which a 1:1 mixture of BM from either wild-type, UBC-Cre-ERT2;*Zfp574*$^{f/f}$, or Eμ-Myc^{TG};UBC-Cre-ERT2;*Zfp574*$^{f/f}$ mice (CD45.2) and congenic wild-type mice (CD45.1) was transferred to lethally irradiated wild-type CD45.1 recipients (Fig. 4*F*). Twelve weeks after BMT, recipients were administered with a first dose of tamoxifen (Fig. 4*G*; days 0 to 5). Tamoxifen-induced *Zfp574* deletion resulted in more rapid elimination of leukemic B cells (Eμ-Myc^{TG};UBC-Cre-ERT2;*Zfp574*$^{f/f}$) than nonmalignant *Zfp574*-deficient B cells (UBC-Cre-ERT2;*Zfp574*$^{f/f}$; Fig. 4 *G* and *H*). Up to 79.3% of established leukemic B cells were eliminated after

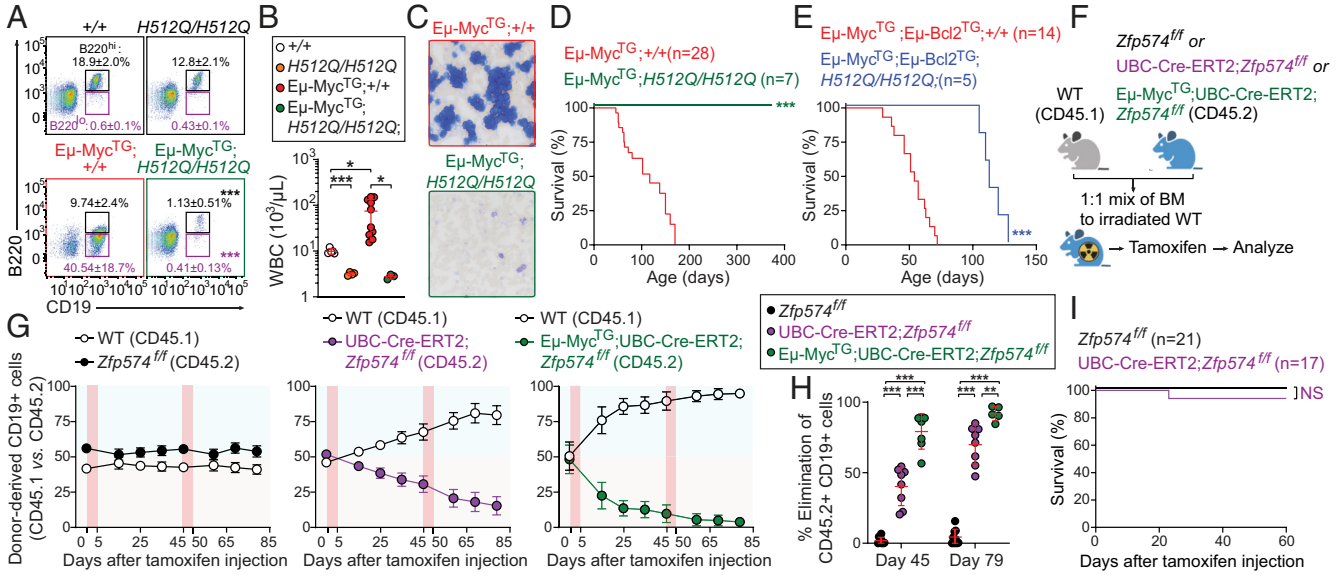

Fig 4. Germline *Zfp574* mutation or tamoxifen-induced *Zfp574* deletion in adult mice suppresses B cell malignancies. (*A*) Representative flow cytometry plots showing the frequency of mature B cells (B220^{high}CD19^{high}) and B lymphoblasts (B220^{lo}CD19^{high}) in the blood of 10-wk-old *Zfp574*$^{H512Q/H512Q}$ or *Zfp574*$^{+/+}$ littermates with or without an Eμ-Myc^{TG} transgene. Numbers adjacent to outlined areas indicate percent cells in each. Disease progression in Eμ-Myc^{TG} mice is manifested by diminished frequencies of mature B220^{hi} B cells and expansion of B220^{lo} leukemic pre-B cells in the peripheral blood; the latter are greatly reduced by the *Zfp574* mutation. (*B*) White blood cell counts in the blood of 8-wk-old *Zfp574*$^{H512Q/H512Q}$ or *Zfp574*$^{+/+}$ littermates with or without an Eμ-Myc^{TG} transgene. (*C*) Representative blood smears showing lymphoblasts in 12-wk-old *Zfp574*$^{+/+}$ or *Zfp574*$^{H512Q/H512Q}$ mice on an Eμ-Myc^{TG} background. (*D* and *E*) Survival curve of Eμ-Myc^{TG} (*D*) or Eμ-Myc^{TG};Eμ-BCL2^{TG} (*E*) mice with wild-type (+/+) or mutant *Zfp574* (*H512Q/H512Q*). (*F*) Approach to test the effect of tamoxifen-induced acute *Zfp574* deletion on established B cell leukemia in adult mice. A 1:1 mixture of *Zfp574*$^{f/f}$, or UBC-Cre-ERT2;*Zfp574*$^{f/f}$, or Eμ-Myc^{TG};UBC-Cre-ERT2;*Zfp574*$^{f/f}$ BM (CD45.2) and congenic WT BM (C57BL/6J; CD45.1) competitor cells were injected into lethally irradiated wild-type CD45.1 recipients. (*G*) Twelve weeks after BM transplantation (day 0), recipients were administered with tamoxifen from days 0 to 5 and 45 to 50 (shaded in red). The frequency of donor-derived CD19+ B cells in the peripheral blood (CD45.1 and CD45.2) was analyzed by flow cytometry until day 79. (*H*) Percentage of donor-derived, tamoxifen responsive nonmalignant (UBC-Cre-ERT2;*Zfp574*$^{f/f}$) or leukemic B cells (Eμ-Myc^{TG};UBC-Cre-ERT2;*Zfp574*$^{f/f}$), or tamoxifen nonresponsive wild-type B cells (*Zfp574*$^{f/f}$) eliminated by the indicated day after the first tamoxifen treatment relative to the number on day 0. (*I*) Survival curve following tamoxifen administration in 10-wk-old UBC-Cre-ERT2;*Zfp574*$^{f/f}$ mice and *Zfp574*$^{f/f}$ littermates. Each symbol represents an individual mouse (*B* and *H*). *P*-values were determined by Student's *t* test (*A*; Eμ-Myc^{TG};*Zfp574*$^{+/+}$ littermates vs. Eμ-Myc^{TG};*Zfp574*$^{H512Q/H512Q}$), one-way ANOVA with Dunnett's multiple comparisons (*B* and *H*) or log-rank test (*D*, *E*, and *I*). Data are representative of one (*D* and *E*), two (*F–I*), or three (*A–C*) independent experiments with 3 to 28 mice per genotype. Error bars indicate SD. *$P < 0.05$; **$P < 0.01$; ***$P < 0.0001$. NS, not significant with $P > 0.05$.

the first dose of tamoxifen, whereas 40.3% of nonmalignant *Zfp574*-deficient B cells were eliminated (Fig. 4 *G* and *H* and *SI Appendix*, Fig. S8*C*; day 45). Since complete excision of the floxed *Zfp574* exon was not achieved by the first dose of tamoxifen (*SI Appendix*, Fig. S8 *A* and *B*), recipients were treated with a second dose of tamoxifen from days 45 to 50. The treatment resulted in elimination of up to 91.9% of leukemic B cells, significantly more than were eliminated among nonmalignant *Zfp574*-deficient B cells (Fig. 4 *G* and *H* and *SI Appendix*, Fig. S8*C*; day 79). Importantly, we found that adult mice survived acute deletion of *Zfp574* (Fig. 4*I*), in contrast with deletion in the zygote (*SI Appendix*, Table S1). Together, these data demonstrate the utility of ZFP574 deletion in suppressing established B cell leukemia in vivo and suggest that ZFP574 disruption throughout the body is tolerated in adult animals.

Establishment of ZFP574 Disruption as a Therapeutic Strategy for B Cell Malignancies. Many transcription factors have proven difficult to target using classical approaches (i.e., small molecules, antibodies, etc.) and are typically considered undruggable. Proteolysis-targeting chimera (PROTAC) or other degradation-based systems harness the ubiquitin–proteasome pathway to degrade specific protein targets in a tunable fashion and have been successfully applied to modulate historically undruggable proteins (20). To examine the efficacy of rapid and reversible ZFP574 degradation in treating established B cell leukemia, we used a degradation tag (dTAG) system in which ZFP574 was C-terminally tagged in the germline with a knock-in of FKBP12^{F36V} followed by a 2X-HA tag (*Zfp574*-FKBP12^{F36V}-HA; Fig. 5*A*). The HA tag was added to monitor ZFP574 degradation. In this system, a dTAG molecule such as dTAG^{V}-1 (21) is used to simultaneously engage ZFP574-FKBP12^{F36V}-HA and the Von Hippel–Lindau (VHL) E3 ligase complex, which ubiquitinates the target, resulting in ZFP574 degradation via proteasomes (Fig. 5*A*).

Following validation of the system (Fig. 5*B*), we administered dTAG^{V}-1 or vehicle control to *Zfp574*-FKBP12^{F36V}-HA homozygotes, Eμ-Myc^{TG};*Zfp574*-FKBP12^{F36V}-HA homozygotes, and wild-type littermates for 4 d. Blood was collected on day 0 (prior to dTAG^{V}-1 injection) and day 4 (12 h after the last dTAG^{V}-1 injection) for FACS analysis. ZFP574 degradation resulted in faster and selective elimination of Eμ-Myc^{TG}-driven established leukemic pre-B cells (B220^{low}CD19^{+}) than nonmalignant B cells (B220^{hi}CD19^{+}; Fig. 5 *C*–*E*). However, dTAG^{V}-1 had no effect on dTAG^{V}-1 nonresponsive wild-type B cells (*Zfp574*$^{+/+}$; Fig. 5*D*). These data provide proof of principle for ZFP574 degradation as a therapeutic approach to preexisting B cell leukemia in vivo.

Discussion

We have investigated the physiological functions of the ZFP574–THAP12 complex, which prior to this work were unknown, likely because of the lack of viable *Zfp574*- or *Thap12*-deficient mouse models. We identified a viable missense mutation of *Zfp574* that impaired hematopoiesis in a cell-intrinsic manner, leading to deficiencies in all immune and blood cell populations. We demonstrated by several approaches the utility of targeting ZFP574 for suppressing B cell leukemia and lymphoma in mice. Genetic deletion or protein degradation of ZFP574 in adult mice eliminated Eμ-Myc^{TG}-driven leukemic B cells preferentially over nonmalignant B cells. Moreover, partial loss-of-function of ZFP574 significantly extended the lifespan of mice with highly aggressive double-hit (Eμ-Myc^{TG};Eμ-BCL2^{TG}) lymphomas. This suggests that targeting ZFP574 may be beneficial for patients with double-hit lymphomas containing translocations increasing the expression of *Myc* and *Bcl2* (or *Bcl6*), which account for ~10% of diffuse large B cell lymphomas (DLBCL) and 30 to 70% of Burkitt lymphomas (22). These patients have a poor prognosis when treated with standard chemotherapy compared to other forms of non-Hodgkin's B cell lymphomas (NHL).

Since ZFP574 functions in HSPC populations to support normal hematopoiesis (Fig. 2), inhibition is expected to cause pan-cytopenia which may be dose-limiting. Based on the observations reported in this paper, we anticipate that targeting the ZFP574–THAP12 complex may elicit a strong therapeutic effect in B cell leukemia with acceptable side effects. Moreover, we anticipate that myeloid

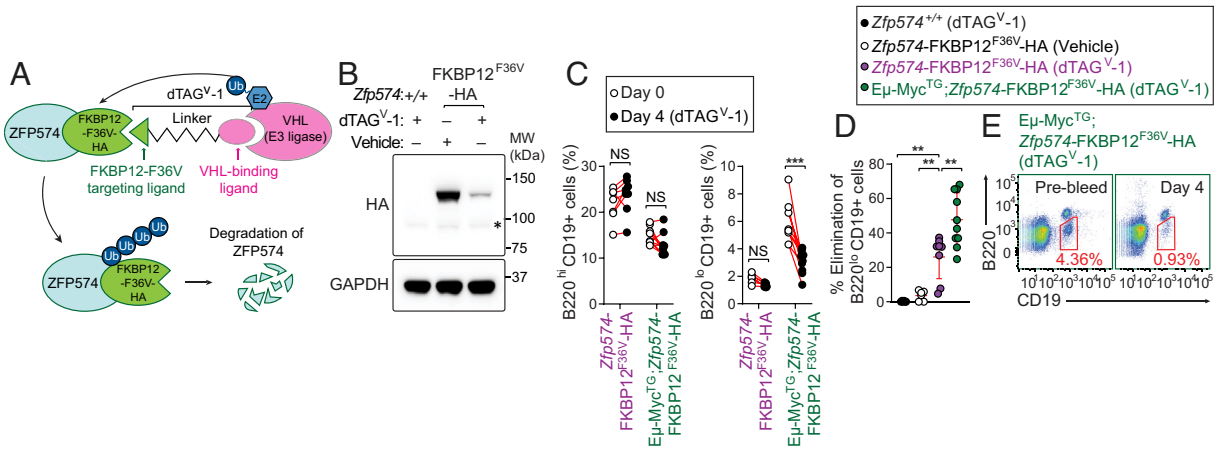

Fig 5. Rapid and reversible ZFP574 degradation suppresses B cell leukemia in mice. (*A*) Schematic of the degradation TAG (dTAG) system designed to selectively degrade endogenous ZFP574 in mice. The dTAG^{V}-1 molecule is used to recruit endogenous ZFP574 tagged with an in-frame germline knock-in of a sequence encoding FKBP12 carrying the substitution F36V to the Von Hippel–Lindau (VHL) E3 ligase complex, which ubiquitinates the target (ZFP574), resulting in its degradation via proteasomes. (*B*–*D*) To test the effect of dTAG^{V}-1-mediated acute ZFP574 degradation in treating established B cell leukemia, 12-wk-old mice were administered with either 5 mg/kg body weight of dTAG^{V}-1 or vehicle control by retro-orbital injection (three times/day for 3 d). (*B*) Splenic B cells were harvested on day 4 from mice with the indicated genotype and treatment and TCL were used to monitor degradation of endogenous ZFP574 by immunoblotting with antibodies against HA. *, an unknown HA-positive protein whose expression is unchanged. GAPDH was used as a loading control. (*C*) Frequencies of B220^{hi} and B220^{low} CD19^{+} B cells in the peripheral blood before (day 0) and after (day 4) dTAG^{V}-1 treatment. (*D*) Percentage of B220^{low}CD19^{+} leukemic pre-B cells in the peripheral blood eliminated by day 4 relative to the number on day 0. Each symbol represents an individual mouse. (*E*) Representative flow cytometry plots showing rapid elimination of leukemic pre-B cells (B220^{low}CD19^{+}) by dTAG^{V}-1 mediated transient ZFP574 degradation in the blood of 12-wk-old *Zfp574-FKBP12*^{F36V}-HA mice on an Eμ-Myc^{TG} background. Numbers adjacent to outlined areas indicate percent cells in each. *P*-values were determined by Student's *t* test (*C*) or one-way ANOVA with Dunnett's multiple comparisons (*D*). Data are representative of two independent experiments with 6 to 10 mice per genotype (*B*–*E*). Error bars indicate SD. $^{**}P < 0.01$.

neoplasms will also respond to drugs targeting the ZFP574–THAP12 complex, and a favorable therapeutic index might be identified for both lymphoid and myeloid lineage diseases.

We showed that THAP12 is the sole interactor with ZFP574 in lymphocytes. While not impacting its cellular abundance or its association with THAP12 in cells, the ZFP574^{H512Q} mutation reduced the amounts of both proteins in the nucleus. Interestingly, the H512Q mutation lies within the sequence of ZFP574 required for interaction with THAP12, but it did not impair binding with THAP12, suggesting that other interaction points may be sufficient to mediate binding. THAP proteins have been shown to bind DNA, but we do not know whether one or both ZFP574 and THAP12 contact DNA directly. Previous reports showed THAP11, ZNF143, and HCF-1 form an interdependent complex that is recruited to chromatin as an intact complex (23). The apparent coregulation of ZFP574 and THAP12 nuclear localization supports the idea that these proteins are recruited to the nucleus and to target DNA as an integral complex. While the mechanism of transcription regulation by ZFP574–THAP12 remains unknown, the absence of an HBM in THAP12 and our interactome studies suggest that it may not involve HCF-1. Regardless, the cell cycle inhibitory and proapoptotic signals resulting from disruption of ZFP574–THAP12 can prevail over oncogenic Myc signaling that promotes protein synthesis and cell cycle progression. The highly proliferative state of leukemic B cells, more of which are proliferating at any given time compared to nonmalignant B cells, may be the reason they are more susceptible to death in the absence of ZFP574 or THAP12.

Materials and Methods

Mice. ENU mutagenesis was performed in pure C57BL/6J male mice as previously described (13, 24). Whole exome sequencing and automated meiotic mapping were conducted following the methods outlined in our earlier publications (13, 25).

Mice carrying targeted missense mutations, null mutations, or insertions in *Zfp574* were generated by CRISPR/Cas9 gene targeting. This was achieved using sgRNA with or without Ultramer oligonucleotide template DNA, as summarized in *SI Appendix*, Table S2. To generate mice expressing 3X-FLAG tag at the C terminus of ZFP574^{WT} or ZFP574^{H512Q} proteins, in vitro fertilization was performed using sperm from male *Zfp574*$^{+/H512Q}$ mice. The *Zfp574*$^{+/H512Q}$ mice had a T to A transversion [AGAAGTCTCA(T)[A]GTGCGGAACCA], resulting in a change of histidine to glutamine at position 512 of 900 amino acids in ZFP574 (NP_780686.1). The founder *Zfp574*^{flox} mice carrying a *lox*P-flanked *Zfp574* exon 2 (containing the entire 2703-bp coding sequence in transcript NM_175477.5) were outcrossed to C57BL/6J mice to confirm 5′ and 3′ *loxP* sites were present on the same chromosome. The founder *Pkr* null mice harbored a 2-bp deletion in exon 2 [TTTCCAGAAG(CC)AAAGGTAGATC], resulting in a frameshift mutation that led to a truncated protein product starting after amino acid 53 of PKR [full length (FL): 515 aa]. The founder *Ceacam*^{S35T} mice carried a T to A transversion [CGACATCGAA(T)[A]CCTTACCACC], resulting in a substitution of serine to threonine at position 35 of CEACAM3. Genotyping was conducted using the primer sets outlined in *SI Appendix*, Table S3.

C57BL/6J (RRID:IMSR_JAX:000664), B6.129P2(C)-*Cd19*$^{tm1(cre)Cgn}$/J (RRID:IMSR_JAX:006785) (Cd19-Cre), B6.Cg-Tg(Cd4-cre)1Cwi/BfluJ (RRID:IMSR_JAX:022071) (Cd4-Cre), B6.Cg-*Ndor1*$^{Tg(UBC-cre/ERT2)1Ejb}$/2J (RRID:IMSR_JAX:008085) (UBC-Cre-ERT2), C57BL/6.SJL (CD45.1), B6.Cg-Tg(BCL2)36Wehi/J (RRID:IMSR_JAX:002321) (Eμ-BCL2^{TG}), B6.Cg-*Rag2*$^{tm1.1Cgn}$/J (RRID:IMSR_JAX:008449) (*Rag2*$^{-/-}$), B6.Cg-Tg(TcraTcrb)425Cbn/J (RRID:IMSR_JAX:004194) (OT-II), and B6.Cg-Tg(IghMyc) 22Bri/J (RRID:IMSR_JAX:002728) (Eμ-Myc^{TG}) mice were purchased from The Jackson Laboratory. *Zfp574*$^{H512Q/H512Q}$, Eμ-Myc^{TG};*Zfp574*$^{H512Q/H512Q}$, Eμ-Myc^{TG}; Eμ-Bcl2^{TG};*Zfp574*$^{H512Q/H512Q}$, Cd19-Cre;*Zfp574*$^{f/f}$, UBC-Cre-ERT2;*Zfp574*$^{f/f}$, Eμ-Myc^{TG};UBC-Cre-ERT2;*Zfp574*$^{f/f}$, *Zfp574*$^{H512Q/H512Q}$;*Pkr*$^{-/-}$, *Zfp574*$^{H512Q/H512Q}$;OT-II, and Eμ-Myc^{TG};*Zfp574*-FKBP12^{F36V}-2X-HA strains were generated through intercrossing of mouse strains. All animal experiments were conducted in accordance with protocols approved by the Institutional Animal Care and Use Committee of the University of Texas Southwestern Medical Center.

Flow Cytometry. As previously described (25–32), peripheral blood was collected and stained with a cocktail of fluorescence-conjugated antibodies targeting 15 cell surface markers across major immune lineages: B220 (BD, clone RA3-6B2), CD19 (BD, clone 1D3), IgM (BD, clone R6-60.2), IgD (BioLegend, clone 11-26c.2a), CD3ε (BD, clone 145-2C11), CD4 (BD, clone RM4-5), CD8α (BioLegend, clone 53-6.7), CD11b (BioLegend, clone M1/70), CD11c (BD, clone HL3), F4/80 (Tonbo, clone BM8.1), CD44 (BD, clone 1M7), CD62L (Tonbo, clone MEL-14), CD5 (BD, clone 53-7.3), CD43 (BD, clone S7), NK 1.1 (BioLegend, clone OK136), and 1:200 Fc block (Tonbo, clone 2.4G2). Data were collected using a BD LSR Fortessa flow cytometer and analyzed with FlowJo software.

Immunization and Enzyme-Linked Immunosorbent Assay (ELISA) Analysis. Immunization and antigen-specific ELISA were conducted as previously described (31, 32). Serum concentrations of IgG1, IgG2a, IgG2b, IgA, IgE, or IgM in naive *Zfp574*$^{H512Q/H512Q}$ and *Zfp574*$^{+/+}$ littermates were analyzed by the ELISA following the manufacturer's instructions (IgG1: Fortis Life Sciences; IgG2a, IgG2b, IgA, IgE, and IgM: Thermo Fisher Scientific).

Hematological Analysis. Hematological parameters of the genetically engineered mouse strains were analyzed with a HemaVet 950FS hematology analyzer (Drew Scientific).

In Vitro Class Switching and Cell Cycle Analysis. As previously described (27, 28), splenic naive B lymphocytes were isolated using CD43 MicroBeads (Miltenyi Biotec). Cells were stained with 5 μM CellTrace CFSE (Life Technologies) and stimulated to undergo class switching to IgG1 with 25 μg/mL LPS (Sigma Aldrich) and 10 ng/mL mouse recombinant IL-4 (BioLegend) for 72 h at 37 °C. For cell cycle analysis, splenic naive B cells or EL4 T cells were stimulated with LPS and IL-4 as described above for 72 h at 37 °C. Subsequently, cells were labeled with the Click-iT EdU Flow Cytometry Assay Kit (Invitrogen) following the manufacturer's instructions. DNA content was analyzed using FxCycle Violet Stain (Invitrogen) by flow cytometry. In vitro class switching and cell cycle progression were assessed using flow cytometry.

Detection of Apoptosis. Annexin V/propidium iodide (PI) labeling was performed using the FITC-Annexin V Apoptosis Detection Kit I (BD Bioscience) following the manufacturer's instructions, and the samples were analyzed by flow cytometry.

Mass Spectrometry Analysis of ZFP574 or THAP12 Interactome. Splenic *Zfp574*$^{FLAG/+}$ B cells and EL4 T cells stably expressing FLAG-tagged ZFP574 or THAP12 were used for immunoprecipitation assays. Immunoprecipitation was carried out with anti-FLAG M2 agarose beads (Sigma) following a standard protocol described in refs. 26, 28, 29, and 31.

As written in our previous papers (27–29), "Immunoprecipitates were precipitated in 23% Trichloroacetic acid at 4 °C overnight and rinsed with cold acetone. Proteins were solubilized in 8 M urea 100 mM Triethylammonium bicarbonate pH 8.5 and reduced with 5 mM Tris (2-carboxyethyl) phosphine hydrochloride (Sigma-Aldrich, product C4706) and alkylated with 55 mM 2-Chloroacetamide (Sigma-Aldrich, product 22790). Proteins were digested for 18 h at 37 °C in 2 M urea 100 mM Triethylammonium bicarbonate pH 8.5, with 0.5 μg trypsin (Promega, Madison, WI, product V5111). A Q Exactive HF Orbitrap Mass Spectrometer (Thermo Scientific) was used for peptide analysis. Protein and peptide identification were done with MSFragger (version 3.4) (33) (https://fragpipe.nesvilab.org/) using a mouse protein database downloaded from UniProt (uniprot.org) (24 November 2023, 21,701 entries), common contaminants and reversed sequences added. The search space included all fully tryptic peptide candidates with a fixed modification of 57.021464 on C, variable modification of 15.9979 on M and 42.0106 on the N terminus. MS1 quantification was done with Total Intensity and no match between runs. Protein intensity values were combined for replicates."

Plasmids. FL mouse ZFP574 (NM_175477.5) or THAP12 (NM_028410.2) with an N-terminal HA tag was cloned into pCMV6 vector. FL mouse ZFP574^{H512Q}, ZFP574 truncated forms (ZFP574$^{39-900}$, ZFP574$^{99-900}$, ZFP574$^{149-900}$, ZFP574$^{236-900}$, ZFP574$^{335-900}$, ZFP574$^{362-900}$, ZFP574$^{390-900}$, ZFP574$^{417-900}$, ZFP574$^{493-900}$, ZFP574$^{149-848}$, ZFP574$^{149-820}$, ZFP574$^{149-792}$, ZFP574$^{149-764}$, ZFP574$^{149-692}$, ZFP574$^{149-659}$, ZFP574$^{149-633}$, ZFP574$^{149-604}$, ZFP574$^{149-576}$, ZFP574$^{149-548}$, ZFP574$^{149-520}$, ZFP574$^{149-492}$, ZFP574$^{149-416}$, ZFP574$^{149-389}$, ZFP574$^{149-361}$,

ZFP574$^{149-334}$, and ZFP574$^{149-235}$), THAP12^{WT}, and THAP12 truncated forms (THAP12$^{1-150}$, THAP12$^{151-758}$, THAP12$^{208-758}$, THAP12$^{360-758}$, THAP12$^{151-359}$, and THAP12$^{209-359}$) with FLAG epitope were cloned into pCDNA6 vector. All plasmids were sequence confirmed to be free of undesirable mutations.

Cell Culture and Immunoblotting. Basic biochemistry experiments including cell culture, transfection, immunoprecipitation, and immunoblotting were conducted as previously described (26–29, 31, 32). Subcellular fractionation of splenic B cells was performed using the Qproteome Cell Compartment Kit (Qiagen). Immunoblotting utilized the following primary antibodies: FLAG (Sigma Aldrich, clone M2), HA (Cell Signaling Technology, clone C19F4), THAP12 (Bethyl Laboratories, Inc., A300-586A), α-Tubulin (CST, clone DM1A), GAPDH (CST, clone D16H11), Lamin A/C (CST, clone 4C11), and β-Actin (CST, clone 8H10D10). Chemiluminescence signals were visualized using a G:Box Chemi XX6 system (Syngene).

Generation of Thap12$^{-/-}$ EL4 T Cells. Parental EL4 T cells were electroporated with a PX458 plasmid encoding an sgRNA targeting mouse *Thap12* (5′-GCGCTGCCCCCAACTGCACA-3′) and green fluorescent protein (GFP). GFP-expressing EL4 T cells were sorted by FACS and subjected to single colony selection. Individual colonies were screened by immunoblotting using a THAP12 antibody (Bethyl Laboratories, Inc., A300-586A) to select *Thap12$^{-/-}$* EL4 T cells.

Equal numbers of live *Thap12$^{-/-}$* or parental EL4 T cells (1×10^4/well) were seeded in 96-well plates and cultured. Cells were counted every 24 h, and a growth curve was plotted.

Blood Smears. Peripheral blood was used to create thin films on clean glass slides. The blood cells on the slides were fixed in methanol and stained using Wright–Giemsa solution (Sigma–Aldrich). The stained slides were then mounted and dried in the dark.

BM Chimeras. BM chimeras were generated following previously described methods (26, 28, 29, 31, 32). Briefly, lethally irradiated (1,400 rads by gamma irradiation) congenic wild-type (CD45.1) recipients were engrafted with a 1:1 mixture of BM cells from C57BL/6.SJL mice (CD45.1) and *Zfp574$^{f/f}$* (CD45.2), UBC-Cre-ERT2;*Zfp574$^{f/f}$* (CD45.2), or Eμ-Myc^{TG};UBC-Cre-ERT2;*Zfp574$^{f/f}$* (CD45.2) donors. Recipients were maintained on antibiotic water for 4 wk postengraftment. Twelve weeks after reconstitution, blood chimerism was determined using flow cytometry with fluorescence-conjugated antibodies against the CD45 congenic markers [CD45.1 (BioLegend, cloneA10), CD45.2 (BioLegend, clone 104)]. To induce Cre-mediated deletion of *Zfp574*, tamoxifen (Sigma, T5648; 75 mg/kg body weight) was administered intraperitoneally to recipients daily for 5 d.

Administration of dTAG^{V}-1 for Degradation of Endogenous ZFP574 In Vivo. As previously described (21), dTAG^{V}–1 was dissolved in DMSO and then diluted with 5% Kolliphor® HS 15 (Sigma): 0.9% sterile saline (w:v) with the final formulation containing 5% DMSO. The dTAG^{V}–1 solution was stored at 4 °C for the duration of injections. In our experiments with tamoxifen-induced acute *Zfp574* deletion in mice, it takes about 4 to 7 d for the mice to develop pan-cytopenia after the last tamoxifen injection. Thus, to maintain consistent ZFP574 degradation for at least 3 d, we administered 100 μL of dTAG^{V}–1 (4 mg/kg body weight, retro-orbital injection) or vehicle control three times daily (every 6 h) to *Zfp574*-FKBP12^{F36V}-HA homozygotes, Eμ-Myc^{TG};*Zfp574*-FKBP12^{F36V}-HA homozygotes, and wild-type littermates.

Statistical Analysis. All comparisons of differences between two or more groups were analyzed using the statistical tests as indicated, conducted with GraphPad Prism software. Differences with a significance level of $P < 0.05$ were considered statistically significant. P values are denoted as follows: $*P < 0.05$; $**P < 0.01$; $***P < 0.001$; ns, indicating not significant with $P > 0.05$.

Data, Materials, and Software Availability. Raw mass spectrometry data have been deposited in the MassIVE repository with Accession No. MSV000094527 [https://massive.ucsd.edu/ProteoSAFe/dataset.jsp?accession=MSV000094527; (34)]

ACKNOWLEDGMENTS. We acknowledge support from the University of Texas Southwestern Medical Center Proteomics and Transgenic Core facilities for assistance with proteomics experiments and generation of engineered mouse models, respectively. This work was supported by the NIH (AI125581 and CA258602 to B.B.).

1. M. Berg *et al.*, Distinct high resolution genome profiles of early onset and late onset colorectal cancer integrated with gene expression data identify candidate susceptibility loci. *Mol. Cancer* **9**, 100 (2010).
2. J. Zhang, X. Wu, L. Huang, ZNF574 promotes ovarian cancer cell proliferation and migration through regulating AKT and AMPK signaling pathways. *Ann. Clin. Lab Sci.* **52**, 611–620 (2022).
3. H. S. Cheong *et al.*, Epigenetic modification of retinoic acid-treated human embryonic stem cells. *BMB Rep.* **43**, 830–835 (2010).
4. C. J. Bult, P. W. Sternberg, The alliance of genome resources: Transforming comparative genomics. *Mamm. Genome* **34**, 531–544 (2023).
5. L. Du *et al.*, Rumba and Haus3 are essential factors for the maintenance of hematopoietic stem/progenitor cells during zebrafish hematopoiesis. *Development* **138**, 619–629 (2011).
6. A. Sabogal, A. Y. Lyubimov, J. E. Corn, J. M. Berger, D. C. Rio, THAP proteins target specific DNA sites through bipartite recognition of adjacent major and minor grooves. *Nat. Struct. Mol. Biol.* **17**, 117–123 (2010).
7. T. Clouaire *et al.*, The THAP domain of THAP1 is a large C2CH module with zinc-dependent sequence-specific DNA-binding activity. *Proc. Natl. Acad. Sci. U.S.A.* **102**, 6907–6912 (2005).
8. M. Roussigne *et al.*, The THAP domain: A novel protein motif with similarity to the DNA-binding domain of P element transposase. *Trends Biochem. Sci.* **28**, 66–69 (2003).
9. H. Dehaene, V. Praz, P. Lhote, M. Lopes, W. Herr, THAP11F80L cobalamin disorder–associated mutation reveals normal and pathogenic THAP11 functions in gene expression and cell proliferation. *PLoS ONE* **15**, e0224646 (2020).
10. M. Gale Jr. *et al.*, Regulation of interferon-induced protein kinase PKR: Modulation of P58IPK inhibitory function by a novel protein, P52rIPK. *Mol. Cell Biol.* **18**, 859–871 (1998).
11. H. Now, J. Y. Yoo, A protein-kinase, IFN-inducible double-stranded RNA dependent inhibitor and repressor of p58 (PRKRIR) enhances type I IFN-mediated antiviral response through the stability control of RIG-I protein. *Biochem. Biophys. Res. Commun.* **413**, 487–493 (2011).
12. A. S. Hidmark *et al.*, Humoral responses against coimmunized protein antigen but not against alphavirus-encoded antigens require alpha/beta interferon signaling. *J. Virol.* **80**, 7100–7110 (2006).
13. T. Wang *et al.*, Real-time resolution of point mutations that cause phenovariance in mice. *Proc. Natl. Acad. Sci. U.S.A.* **112**, E440–449 (2015).
14. T. Schmitter, F. Agerer, L. Peterson, P. Munzner, C. R. Hauck, Granulocyte CEACAM3 is a phagocytic receptor of the innate immune system that mediates recognition and elimination of human-specific pathogens. *J. Exp. Med.* **199**, 35–46 (2004).
15. T. Groza *et al.*, The International Mouse Phenotyping Consortium: Comprehensive knockout phenotyping underpinning the study of human disease. *Nucleic Acids Res.* **51**, D1038–D1045 (2023).
16. M. Varadi *et al.*, AlphaFold Protein Structure Database: Massively expanding the structural coverage of protein-sequence space with high-accuracy models. *Nucleic Acids Res.* **50**, D439–D444 (2022).
17. J. M. Suski, M. Braun, V. Strmiska, P. Sicinski, Targeting cell-cycle machinery in cancer. *Cancer Cell* **39**, 759–778 (2021).
18. A. W. Harris *et al.*, The E mu-myc transgenic mouse. A model for high-incidence spontaneous lymphoma and leukemia of early B cells. *J. Exp. Med.* **167**, 353–371 (1988).
19. A. Strasser, A. W. Harris, M. L. Bath, S. Cory, Novel primitive lymphoid tumours induced in transgenic mice by cooperation between myc and bcl-2. *Nature* **348**, 331–333 (1990).
20. M. Bekes, D. R. Langley, C. M. Crews, PROTAC targeted protein degraders: The past is prologue. *Nat. Rev. Drug Discov.* **21**, 181–200 (2022).
21. B. Nabet *et al.*, Rapid and direct control of target protein levels with VHL-recruiting dTAG molecules. *Nat. Commun.* **11**, 4687 (2020).
22. J. W. Friedberg, Double hit diffuse large B-cell lymphomas: Diagnostic and therapeutic challenges. *Chin. Clin. Oncol.* **4**, 9 (2015).
23. J. B. Parker, H. Yin, A. Vinckevicius, D. Chakravarti, Host cell factor-1 recruitment to E2F-bound and cell-cycle-control genes is mediated by THAP11 and ZNF143. *Cell Rep.* **9**, 967–982 (2014).
24. P. Georgel, X. Du, K. Hoebe, B. Beutler, ENU mutagenesis in mice. *Methods Mol. Biol.* **415**, 1–16 (2008).
25. D. Xu *et al.*, Thousands of induced germline mutations affecting immune cells identified by automated meiotic mapping coupled with machine learning. *Proc. Natl. Acad. Sci. U.S.A.* **118**, e2106786118 (2021).
26. X. Zhong *et al.*, Genetic and structural studies of RABL3 reveal an essential role in lymphoid development and function. *Proc. Natl. Acad. Sci. U.S.A.* **117**, 8563–8572 (2020).
27. X. Zhong *et al.*, Viable mutations of mouse midnolin suppress B cell malignancies. *J. Exp. Med.* **221**, e20232132 (2024).
28. X. Zhong *et al.*, Essential requirement for IER3IP1 in B cell development. *Proc. Natl. Acad. Sci. U.S.A.* **120**, e2312810120 (2023).
29. X. Zhong *et al.*, Essential role of MFSD1-GLMP-GIMAP5 in lymphocyte survival and liver homeostasis. *Proc. Natl. Acad. Sci. U.S.A.* **120**, e2314429120 (2023).
30. X. Zhong *et al.*, RNPS1 inhibits excessive tumor necrosis factor/tumor necrosis factor receptor signaling to support hematopoiesis in mice. *Proc. Natl. Acad. Sci. U.S.A.* **119**, e2200128119 (2022).
31. J. H. Choi *et al.*, LMBR1L regulates lymphopoiesis through Wnt/beta-catenin signaling. *Science* **364**, eaau0812 (2019).
32. J. H. Choi *et al.*, Essential requirement for nicastrin in marginal zone and B-1 B cell development. *Proc. Natl. Acad. Sci. U.S.A.* **117**, 4894–4901 (2020).
33. A. T. Kong, F. V. Leprevost, D. M. Avtonomov, D. Mellacheruvu, A. I. Nesvizhskii, MSFragger: Ultrafast and comprehensive peptide identification in mass spectrometry-based proteomics. *Nat. Methods* **14**, 513–520 (2017).
34. X. Zhong *et al.*, Therapeutic targeting of ZFP574–THAP12 complex suppresses B cell malignancies in mice. MassIVE. https://massive.ucsd.edu/ProteoSAFe/dataset.jsp?accession=MSV000094527. Deposited 12 April 2024.